

Onboard MuJoCo-based Model Predictive Control for Shipboard Crane with Double-Pendulum Sway Suppression

Oscar Pang[†], Lisa Coiffard[†], Paul Templier[†], Luke Beddow[†], Kamil Dreczkowski[†], Antoine Cully[†]

Abstract—Transferring heavy payloads in maritime settings relies on efficient crane operation, limited by hazardous double-pendulum payload sway. This sway motion is further exacerbated in offshore environments by external perturbations from wind and ocean waves. Manual suppression of these oscillations on an underactuated crane system by human operators is challenging. Existing control methods struggle in such settings, often relying on simplified analytical models, while deep reinforcement learning (RL) approaches tend to generalise poorly to unseen conditions. Deploying a predictive controller onto compute-constrained, highly non-linear physical systems without relying on extensive offline training or complex analytical models remains a significant challenge. Here we show a complete real-time control pipeline centered on the MuJoCo MPC framework that leverages a cross-entropy method planner to evaluate candidate action sequences directly within a physics simulator. By using simulated rollouts, this sampling-based approach successfully reconciles the conflicting objectives of dynamic target tracking and sway damping without relying on complex analytical models. We demonstrate that the controller can run effectively on a resource-constrained embedded hardware, while outperforming traditional PID and RL baselines in counteracting external base perturbations. Furthermore, our system demonstrates robustness even when subjected to unmodeled physical discrepancies like the introduction of a second payload.

I. INTRODUCTION

Maritime crane operations face a persistent challenge: payload sway induced by the coupled effects of crane arm acceleration and continuous base perturbations from ocean waves. This sway frequently manifests as double-pendulum motion, where the payload oscillates both from the boom tip and about the hook-cable connection [1]. The highly non-linear, underactuated nature of these dynamics makes manual stabilization difficult, degrading positioning accuracy and extending task completion times [2]. In the shipboard crane setting, ship-motion-induced disturbances further amplify payload swing, posing risks to the payload and surrounding equipment, and limiting operational efficiency [3]. Suppressing these oscillations in real-time¹ requires a controller that can anticipate disturbances while managing the competing demands of fast payload transfer and sway minimization.

The field of crane anti-sway control is mature and well-studied [2], with approaches spanning input shaping [1], linear

^{*}This work is funded by the Defense Advanced Research Projects Agency (DARPA) Learning Introspective Control (LINC) program.

[†]The authors are with the Adaptive and Intelligent Robotics Lab, Department of Computing, Imperial College London, Exhibition Rd, London, SW7 2BX, United Kingdom

Corresponding authors: Oscar Pang (k.pang@imperial.ac.uk) and Antoine Cully (a.cully@imperial.ac.uk).

¹We use *real-time* in the operational sense of [4]: the planner produces updated policies within a single control cycle, enabling continuous closed-loop operation without offline computation.

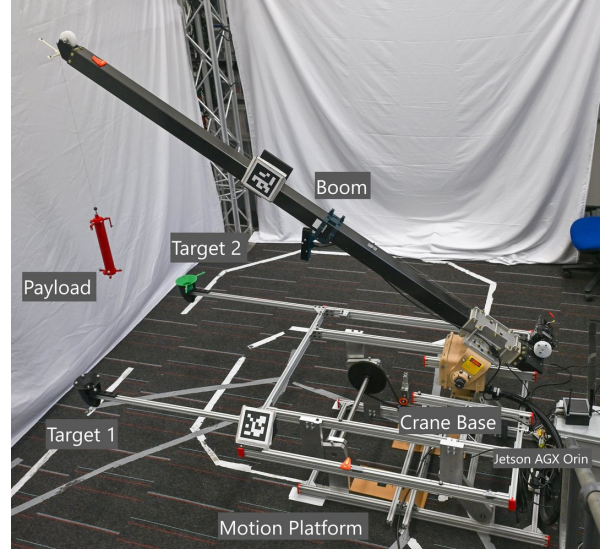


Fig. 1: Experimental setup of a boom-type crane mounted on a motion platform.

and non-linear feedback [5], [6] and model predictive control (MPC) [7], [8], [9]. These share a common dependency on analytically derived equations of motion, typically linearized or reduced in degrees-of-freedom (DoF) to remain computationally tractable [2], [3], [10]. For shipboard cranes under persistent base perturbations, these simplifications are particularly limiting: they discard coupled slew-luff dynamics, double-pendulum dynamics, or non-linear terms that dominate the system response in rough seas [3]. Reinforcement learning (RL) sidesteps the modeling burden but substitutes it with extensive offline training that generalizes poorly to unseen conditions [11].

Recent advances in robotics have demonstrated that general purpose physics simulators can serve as planning models for real-time decision-making. A growing body of work treats the simulator itself as the dynamics model within an MPC loop, where candidate action sequences are evaluated by rolling them forward through the physics engine and the best-performing sequence is executed on hardware [4]. This simulation-based planning paradigm has produced impressive results on different types of robotic platforms, for example, legged locomotion [12], [13] and dexterous manipulation [14], [15]. Nonetheless, the adoption of simulation-based planning has been limited to platforms where high-fidelity models with calibrated actuator dynamics are readily available [16], [17].

We extend this paradigm to shipboard crane control, where three challenges absent from prior simulation-based MPC

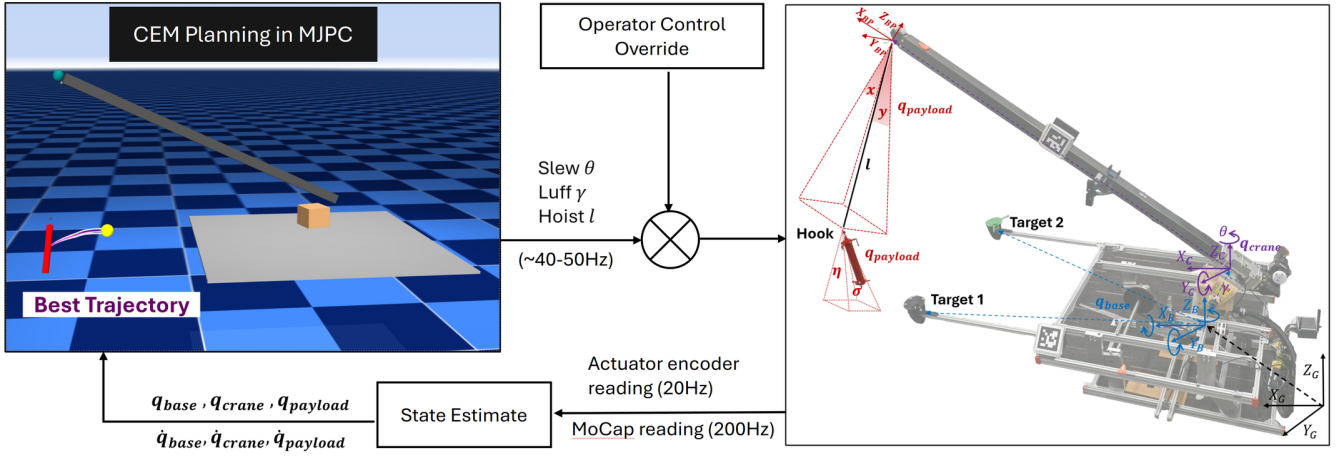


Fig. 2: MJPC controller architecture.

deployments converge: no simulation model exists for the proprietary industrial actuators, the system is underactuated under persistent base perturbations that couple directly into the unactuated payload dynamics, and fast payload transfer inherently conflicts with sway suppression. To address these, we introduce a predictive control pipeline centered on the MuJoCo MPC [4] framework that pairs a system identification workflow with a CEM planner evaluating candidate action sequences through forward rollouts of the full coupled dynamics. This sidesteps the linearization and DoF reduction that existing crane MPC methods require, while an adaptive cost function reconciles the competing demands of target tracking and sway suppression by shifting priorities with proximity to the goal. We validate the complete pipeline on physical hardware under persistent base perturbations, including deployment on an embedded platform NVIDIA Jetson AGX Orin.

Our contributions are as follows:

- 1) We present an alternative approach to analytical-model MPC by managing full double-pendulum dynamics through simulation and sampling-based optimization. This sidesteps the need for linearization, DoF reduction, or the planner–stabilizer decomposition typically required by existing crane control methods.
- 2) We establish a practical example of adopting our approach on a physical crane system. We benchmark our approach against PID and RL baselines to highlight its advantage in reconciling operator intent (transferring a payload to target) with active sway damping on the payload across multiple simulated sea state conditions.
- 3) We provide an analysis on the trade-off between CEM iteration budget and real-time control frequency for deployment on the resource constrained compute platform to achieve real-time control.

II. BACKGROUND

A. Problem Formulation

We consider a boom-type crane with three actuated joints: slew (rotation θ about the vertical axis), luff (boom elevation

angle γ), and hoist (cable length l) mounted on a motion platform, pictured in Fig. 2. The motion platform simulates shipboard motion at sea, which we assume to be periodic and of fixed amplitude, by generating disturbances to the crane base. We suspend a rigid payload of mass m from the boom tip that exhibits double-pendulum dynamics – it can swing freely from both the boom tip and the hook connecting it to the cable.

The complete system state $\mathbf{x}_t = [\mathbf{q}^\top, \dot{\mathbf{q}}^\top]^\top \in \mathbb{R}^{26}$ comprises 13 generalized positions and their velocities:

$$\mathbf{q} = \begin{bmatrix} \mathbf{q}_{\text{base}} \\ \mathbf{q}_{\text{crane}} \\ \mathbf{q}_{\text{payload}} \end{bmatrix} \in \mathbb{R}^{13} \quad (1)$$

where $\mathbf{q}_{\text{base}} = [q_{\text{surge}}, q_{\text{sway}}, q_{\text{heave}}, q_{\text{roll}}, q_{\text{pitch}}, q_{\text{yaw}}]^\top \in \mathbb{R}^6$ represents the platform pose, $\mathbf{q}_{\text{crane}} = [q_{\text{slew}}, q_{\text{luff}}, q_{\text{hoist}}]^\top \in \mathbb{R}^3$ denotes the actuated crane joints and $\mathbf{q}_{\text{payload}} \in \mathbb{R}^4$ denotes double-pendulum swing angle at the boom tip and payload hook. Velocities $\dot{\mathbf{q}} \in \mathbb{R}^{13}$ follow the same decomposition. Of the 13 position coordinates, only $\mathbf{q}_{\text{crane}}$ are directly actuated; the base motion acts as a measured disturbance and the payload states are unactuated.

The primary control challenge lies in the coupling between the actuated crane joints and the unactuated double-pendulum payload joints, exacerbated by continuous energy injection from the base disturbances.

B. Sampling-Based Model Predictive Control

We formulate the task of target tracking and payload sway damping as an optimal control problem over a receding horizon H . The objective is to find a sequence of control actions $\mathbf{u}_{t:t+H}^* = \{\mathbf{u}_t, \dots, \mathbf{u}_{t+H}\}$ that minimizes a cumulative cost:

$$\begin{aligned} \mathbf{u}_{t:t+H}^* &= \arg \min_{\mathbf{u}_{t:t+H}} \sum_{k=0}^{H-1} c(\mathbf{x}_{t+k}, \mathbf{u}_{t+k}) + c_f(\mathbf{x}_{t+H}) \\ \text{subject to} & \quad \mathbf{x}_{t+k+1} = f(\mathbf{x}_{t+k}, \mathbf{u}_{t+k}), \\ & \quad \mathbf{u}_{\min} \leq \mathbf{u}_{t+k} \leq \mathbf{u}_{\max}, \\ & \quad \mathbf{x}_t = \hat{\mathbf{x}}(t). \end{aligned} \quad (2)$$

Following prior applications of simulation-based planning for control of physical hardware [14], we adopt a sampling-based predictive control approach on (2). Unlike gradient-based MPC which requires differentiable dynamics, sampling-based methods like the cross-entropy method (CEM) [18] treat the simulator as a black box: candidate action sequences are evaluated through parallelized forward rollouts with no smoothness requirement on the dynamics or cost.

Our implementation utilizes the CEM planner provided in the MJPC framework to manage these rollouts asynchronously, as outlined in Algorithm 1. At each time t , the planner receives a state estimate $\hat{\mathbf{x}}(t)$ and samples a batch of N control trajectories from a parametric distribution $\pi_{\theta}(\mathbf{U})$ - typically a diagonal Gaussian $\mathcal{N}(\boldsymbol{\mu}, \boldsymbol{\Sigma})$. These trajectories are represented as splines with K knots, which serve as the decision variables for the optimization.

Algorithm 1 Cross-Entropy Method for Online Planning

Require: Parameters $\theta = (\boldsymbol{\mu}, \boldsymbol{\Sigma})$, sample size N , elite count M

- 1: **while** planning **do**
- 2: $\hat{\mathbf{x}}_t \leftarrow \text{GetStateEstimate}(t)$
- 3: // Sampling and Rollout
- 4: **for** $i = 1$ **to** N **do**
- 5: $\mathbf{U}^{(i)} \sim \mathcal{N}(\boldsymbol{\mu}, \boldsymbol{\Sigma})$ {Generate candidate trajectory}
- 6: $J^{(i)} \leftarrow \text{Simulate}(\mathbf{U}^{(i)}, \hat{\mathbf{x}}_t)$ {Evaluate Eq. (2) via MuJoCo}
- 7: **end for**
- 8: // Evaluation and Selection
- 9: $\mathcal{E} \leftarrow \{\mathbf{U}^{(i)}\}_{i=1}^M$ s.t. $J^{(i)}$ are the M lowest costs
- 10: $\mathbf{U}^* \leftarrow \arg \min_{\mathbf{U} \in \mathcal{E}} J(\mathbf{U})$ {Best candidate trajectory}
- 11: // Distribution Update
- 12: $\boldsymbol{\mu} \leftarrow \frac{1}{M} \sum_{\mathbf{U} \in \mathcal{E}} \mathbf{U}$
- 13: $\boldsymbol{\Sigma} \leftarrow \frac{1}{M} \sum_{\mathbf{U} \in \mathcal{E}} (\mathbf{U} - \boldsymbol{\mu})(\mathbf{U} - \boldsymbol{\mu})^\top$
- 14: // Update Nominal Policy
- 15: $\boldsymbol{\pi}^* \leftarrow \mathbf{U}^*$
- 16: // Asynchronous Action Application
- 17: $\mathbf{u}_t \leftarrow \text{Interpolate}(\boldsymbol{\pi}^*, t)$ {First action from best trajectory}
- 18: **end while**

III. RELATED WORK

A. Classical and Adaptive Anti-Sway Crane Control

Crane control has been studied extensively, from open-loop filtering to closed-loop feedback strategies [2]. Open-loop methods such as input shaping [1] generate reference commands designed to cancel the payload’s natural oscillatory modes, and hybrid schemes [19], [20] combine input shaping with closed-loop MPC to improve robustness. However, these remain limited in offshore settings, where wave motion continuously injects energy into the payload dynamics after the command is shaped.

Closed-loop strategies better address the double-pendulum effect and parametric uncertainties. non-linear control [5], sliding mode control [21], and Lyapunov-based adaptive

strategies [6], [22], [23] offer formal guarantees on transient performance, ensuring that payload swing and tracking errors converge within predefined bounds despite varying cable lengths. However, these methods are primarily **reactive**; they suppress sway only after it manifests in the system state.

Conversely, MPC enables **anticipatory** disturbance rejection by optimizing control actions over a receding horizon. However, applying MPC to crane systems with coupled, non-linear dynamics requires simplifications to ensure the online optimization problem remains tractable. Existing literature addresses this through three primary strategies. The first is *linearization*, where dynamics are approximated along a reference path [24] or via successive Taylor-series expansions to formulate convex sub-problems [5]. The second strategy, *DoF reduction*, decreases model dimensionality by omitting specific axes (such as the slew angle) [25] or by decoupling unactuated dynamics from actuated states [7]. The third strategy is *problem decomposition*, which separates control objectives [26]. Even data-driven variants [27], which sidestep analytical derivation, rely on identified reduced-order models. Consequently, all these approaches achieve real-time computational feasibility by intentionally discarding specific complex interactions, such as coupled slew-luff dynamics, double-pendulum dynamics or non-linear coupling terms.

B. Learning-Based Approaches

Recent literature explores deep reinforcement learning (RL) to capture non-linearities without explicit dynamics modeling. Various works apply RL algorithms, such as proximal policy optimization (PPO) [28] and soft actor-critic (SAC) [29] for crane control, while Vu et al. [11] benchmark RL algorithms for boom-type forestry crane operation. While promising, these RL-based controllers require extensive offline training, and once deployed, generalize poorly to out-of-distribution scenarios [30]. If environment dynamics change, the policy may require extensive retraining. Our MPC-based approach, by contrast, adapts online via its internal predictive model.

C. Sampling-Based MPC on Robotic Platforms

The use of high-fidelity simulators as real-time synthesis of complex behaviors has gained significant traction in robotics [31], [32], [33], [34]. These approaches leverage parallelized rollouts within physics engines to enable dynamic locomotion and manipulation via sampling-based optimization. Because the simulator implicitly defines the dynamic model, these methods are readily extendable to diverse objects and morphologies without the extensive offline training required by RL [30].

Within this paradigm, MuJoCo MPC (MJPC) [4] provides an open-source framework for real-time predictive control that leverages high-fidelity physics simulation. Recent works demonstrate its versatility across hardware platforms, from legged locomotion [12] to dexterous manipulation [14], [15].

While previous applications focus largely on fully-actuated or contact-rich systems, we extend this paradigm to the underactuated domain of offshore cranes. We distinguish

TABLE I: Physical parameters of the crane and motion platform

Parameter	Value	Unit
Boom length	2.384	m
Slew range	[−86, 86]	degree
Luff range	[0, 54.4]	degree
Hoist cable range	[0.07, 2.0]	m
Slew speed limit	±52.7	degree/s
Luff speed limit	±27.5	degree/s
Hoist speed limit	±1.0	m/s
Payload mass	0.317	Kg
Payload dimensions	∅50×460	mm
Base x, z displacement	0.18, 0.04	m
Base pitch angle	[−9.3, 7.5]	degree
Period (SLOW / MEDIUM / FAST)	12 / 7 / 5	s

TABLE II: Identified actuator and joint parameters

Joint	K_v	u	I_{arm}	Damping
Slew	7800	±0.92	1000	0.01
Luff	13000	±0.48	2200	0.01
Hoist [†]	25000	±1.0	3200	0.0

[†]Friction loss = 30 to prevent payload slip.

our work by addressing the unique challenge of double-pendulum sway suppression, demonstrating that sampling-based MPC can effectively reconcile competing objectives (payload transfer and sway damping), while handling the non-linear dynamics induced by external wave disturbances.

IV. METHOD

A. Modeling and System Identification

We model the crane system from Fig. 1 in MuJoCo using the physical parameters of the experimental setup, detailed in Table I. This simulated model serves as the forward dynamics model $f(\cdot)$ (see Eq. (2)) in MJPC.

The three actuated crane joints $\mathbf{q}_{\text{crane}}$ are modelled as velocity actuators with gain K_v and velocity range u . Each joint also has an armature I_{arm} , which represents the rotor inertia of the actuators. We model the cable connecting the crane’s boom tip to the payload with a prismatic slider joint of variable length l , under the assumption that it remains taut. This avoids using a cable or rope in the simulator, which increases computation. For $\mathbf{q}_{\text{payload}}$, we add two pairs of orthogonal hinge joints to the boom tip and payload hook that simulate the payload’s double-pendulum behavior. Finally, we model \mathbf{q}_{base} as six-DoF position actuators at the crane base, enabling the planner to anticipate measured periodic excitation during rollouts.

We tune K_v and I_{arm} parameters in two stages: (1) we adjust K_v to match the commanded steady-state velocity and (2) we tune I_{arm} to match the transient response slope during acceleration and deceleration. We validate these parameters by computing the root-mean-square error between real and simulated poses of the crane over the full excitation sequence. We summarize identified parameters in Table II.

B. Cross-Entropy Method for Model Predictive Control

1) *Cross-Entropy Method for Real-Time Control*: The CEM planner has a prediction horizon of 0.8 s. In our exper-

TABLE III: CEM hyperparameter values

Parameter	Value
Horizon length (H)	0.8 s
Model time-step (Δt)	0.01 s
Planner iterations	5
Trajectory sample size (N)	20
Elite count (M)	5
Sampling noise (σ)	0.2
No. of spline knots (K)	3
Spline representation	Zero-order hold

iments, extending the horizon beyond this value yielded no measurable improvement in sway damping while significantly reducing the replanning frequency. The planner simulates 20 candidate trajectories in parallel, selecting five elites with the lowest cost to refit the sampling distribution over subsequent planning iterations, as outlined in Algorithm 1. We restrict the sampling distribution to the three crane actuators (slew, luff and hoist). The six base DoF are not optimized but instead prescribed from the disturbance prediction module (Section IV-C), reducing the planner’s search space. In each planning cycle, the CEM planner runs five planning iterations to improve the policy before executing the first action of the best trajectory \mathbf{u}_t^* on the physical system. We provide an overview of CEM hyperparameters in Table III.

2) *Cost Function Design*: The cost function must reconcile two competing objectives [6]: accurately tracking a moving target and maintaining minimal payload oscillation over the target position. The individual cost terms are detailed in Table IV.

To ensure smooth station-keeping, r_{target} employs a Pseudo-Huber norm. Its flat region near zero suppresses actuator jitter once the payload is within an acceptable tolerance of the goal, where positioning is de-prioritized in favor of active sway damping. Oscillation metrics like sway r_{sway} and payload tilt r_{tilt} grow linearly to prevent disproportionate or destabilizing corrective effort during large transient swings. The quadratic norm applied to r_{vel} and r_{ctrl} penalizes unsafe magnitudes super-linearly.

A fixed weighting of all five terms cannot simultaneously satisfy both objectives: emphasizing r_{target} and r_{sway} achieves station-keeping but causes overshoot on a moving target, while emphasizing r_{vel} prevents overshoot but produces heavy oscillations. We resolve this with a distance-dependent tanh blend to dynamically adjust the weights α and β in Table IV. This acts as a continuous relaxation of discrete cost-function switching [31]. Let $d = \|\mathbf{p}_{\text{target}} - \mathbf{p}_{\text{payload}}\|$ be the current distance to the target. The blending coefficients are defined as:

$$\alpha(d) = \frac{1}{2} (\tanh(k_d (d - d_{\text{th}})) + 1), \quad (3)$$

$$\beta(d) = \frac{1}{2} (\tanh(-k_e (d - d_{\text{th}})) + 1) + 1, \quad (4)$$

where $d_{\text{th}} = 0.1$ m is the proximity threshold and $k_d = 10$, $k_e = 5$ control transition sharpness. Far from the target ($d \gg d_{\text{th}}$, $\alpha \rightarrow 1$, $\beta \rightarrow 1$), r_{target} and r_{sway} dominate to guide the payload while suppressing oscillations. Inside the proximity

TABLE IV: Cost function terms

Term	Formulation	Weight
r_{target} : target tracking	$\sqrt{\ \mathbf{p}_{\text{payload}} - \mathbf{p}_{\text{target}}\ ^2 + \varepsilon^2} - \varepsilon$ with $\varepsilon = 0.05$	$A\alpha(d)$
r_{sway} : sway damping	$\sqrt{ \theta_{\text{sway}} ^2 + \delta^2}$ with $\delta = 2.0$	$\frac{A}{2}\alpha(d)$
r_{vel} : relative velocity	$\ \dot{\mathbf{p}}_{\text{payload}} - \dot{\mathbf{p}}_{\text{platform}}\ ^2$	$B\beta(d)$
r_{ctrl} : control effort	$\ \ddot{\mathbf{u}}_{\text{slew}}\ ^2, \ \ddot{\mathbf{u}}_{\text{luff}}\ ^2$	1
r_{tilt} : payload tilt	$\sqrt{ 2\arccos(\mathbf{q}_{\text{payload}} \cdot \mathbf{q}_t) ^2 + \delta^2}$ with $\delta = 3.0$	500

Note: $\theta_{\text{sway}} = \arcsin(\frac{\sqrt{d_x^2 + d_y^2}}{\|\mathbf{b}\|})$ where \mathbf{b} is the boom-tip-to-payload vector.
 $A = 200, B = 350$.

region ($d < d_{\text{th}}, \alpha \rightarrow 0, \beta \rightarrow 2$), emphasis shifts to velocity matching, decelerating the payload to prevent overshoot.

C. State Estimation and Disturbance Prediction

Our state estimation pipeline consists of two parts: instantaneous estimation of the crane-payload system state and prediction of the moving platform’s pose (1). We obtain crane joint angles $\mathbf{q}_{\text{crane}}$ from actuator encoders at 20 Hz. We measure payload angles $\mathbf{q}_{\text{payload}}$ with a motion capture system at 100 Hz, which provides reliable ground-truth pose estimation. We compute joint velocities by applying a 10-step moving average filter to the finite-differenced positions.

To account for anticipated platform movement in planning, we inject predicted base poses into the MuJoCo forward dynamics engine. This allows us to bypass the need for complex, analytical disturbance modeling. We treat the perturbations to the crane base \mathbf{q}_{base} , introduced by the motion platform, as periodic trajectories. We forecast this movement via autocorrelation-based pattern matching over a two-period long sliding window of motion capture data of \mathbf{q}_{base} . This module outputs a prediction of the future base pose sequence, $\{\mathbf{q}_{\text{base}}(t+k)\}_{k=0}^H$, over the entire horizon length H . To prevent prediction drift, we correct residual prediction errors at each re-planning cycle by updating the instantaneous state and disturbance estimates.

V. EXPERIMENTAL SETUP

A. Hardware Setup

We perform all experiments on the setup pictured in Fig. 1 over a range of motion platform speeds (see Table I): STATIC (stationary), SLOW, MEDIUM and FAST. The crane system receives slew, luff and hoist commands at a control frequency of 20 Hz, using ROS. To demonstrate the feasibility of our MJPC controller across different compute regimes, we run it on two platforms: (1) a high-performance laptop (Intel Core i9-12900HK CPU) and (2) an edge computing module (NVIDIA Jetson AGX Orin 64GB). The planning frequency operates at ~ 50 Hz on the laptop versus ~ 40 Hz on the Jetson AGX Orin.

B. Baselines

We evaluate our MJPC controller against a classical baseline (PID) and a learning-based baseline (RL).

Proportional-integral-derivative (PID). We implement a PID controller for simultaneous target position tracking and payload sway damping. The controller combines a PD loop for joint position tracking with a nested PID loop dedicated to payload sway damping for slew, luff and hoist actuator. This represents a reactive classical baseline that lacks the predictive horizon of our approach.

Proximal policy optimization (PPO). As a representative of model-free learning-based methods, we train a PPO [35] agent. To ensure a fair comparison, we train the agent using the same MuJoCo XML model as the MJPC controller with parameters in Table I and Table II. The agent receives a history of five time steps of system state in (1), and publishes the slew, luff and hoist command at the frequency of 50 Hz. The policy uses three hidden layers of 256 neurons, trained in simulation to navigate the payload to a target position subject to random payload disturbances.

In preliminary experiments, we tested two reward designs: one following the cost function from Section IV-B.2, as well as a handcrafted reward penalizing payload distance from the target and acceleration. Across 10 seeds each, we observed that all policies converged to “bang-bang” control, outputting actions of maximum -1 and $+1$ velocity. While this strategy performed well on the simulated task, deployment on the real crane proved unstable, demonstrating progressively increasing oscillations. In our final experiments, we scale actions by 0.25 to mitigate this effect and deploy the best performing policy, using our handcrafted reward.

We report statistical significance for numerical values using Mann-Whitney U tests [36].

VI. RESULTS

We structure our experimental results to address the following research questions.

RQ1: How effectively does our MJPC controller maintain payload stability and tracking accuracy when subjected to external perturbations? **RQ2:** What is the trade-off between CEM planner iterations, action cost convergence and planning frequency, and how does this dictate the feasibility of real-time MJPC deployment, in line with computational constraints? **RQ3:** How robust is the controller to model discrepancies, and how effectively can the underlying MuJoCo model be dynamically adapted to handle unmodeled hardware conditions?

A. Payload Sway Damping and Target Tracking under Perturbation

To evaluate the performance of our MJPC controller, we design a target switching task using two targets mounted 1 m apart on the motion platform, shown in Fig. 1. Starting over one of the targets, we allow 20 seconds for the controller to reach its new target and damp payload sway, after which we switch targets. We collect data from 10 trajectories between the two targets with a total duration of 200 seconds.

TABLE V: Summary statistics of mean position error and payload tilt over 10 to 20-second interval, over various motion platform settings with aggregated median (interquartile range) over 10 replications; statistically significant least error in bold. In the bottom three rows we report the performance degradation (difference from top row errors) with a double-payload system that is not modeled in MJPC over four replications.

Method	Static		Slow		Medium		Fast	
	Pos (m)	Ang (deg)	Pos (m)	Ang (deg)	Pos (m)	Ang (deg)	Pos (m)	Ang (deg)
RL	0.27 (0.40)	7.85 (3.89)	0.39 (0.19)	9.92 (2.33)	0.47 (0.12)	13.82 (2.80)	0.43 (0.12)	13.25 (2.01)
PID	0.08 (0.03)	1.42 (0.11)	0.22 (0.07)	1.75 (0.78)	0.16 (0.04)	3.66 (0.87)	0.20 (0.18)	3.61 (26.65)
MJPC (ours)	0.03 (0.01)	1.86 (1.32)	0.09 (0.01)	1.51 (0.34)	0.11 (0.02)	1.75 (0.78)	0.11 (0.02)	2.21 (1.24)
MJPC [edge] (ours)	0.03 (0.01)	1.44 (0.77)	0.06 (0.02)	2.15 (0.75)	0.07 (0.02)	2.57 (0.38)	0.10 (0.02)	3.47 (1.02)
RL Δ	0.42	3.04	0.35	3.86	-0.04	0.27	0.48	2.53
PID Δ	0.11	0.22	0.06	0.78	0.15	-1.39	0.13	-0.52
MJPC Δ [edge] (ours)	0.03	2.06	0.17	2.79	0.23	-0.76	0.16	0.28

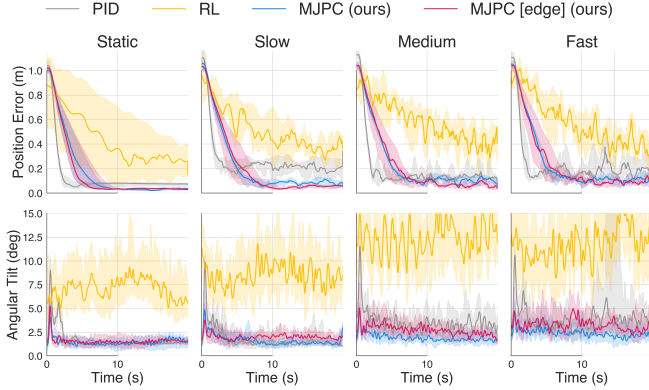


Fig. 3: Payload position error from target (top row) and angular tilt (bottom row) over various motion platform settings. We plot the median (solid line) and IQR (shaded area) over 10 replications.

In Fig. 3, we display aggregated trajectories over all replications of the payload’s xy position error relative to the target (top) and the tilt angle between the payload longitudinal axis and the z -axis of the global frame (bottom). To summarize the controller’s ability to maintain payload stability over the target, Table V aggregates the mean xy position error over the 10 to 20-second interval, once the payload has reached the target.

Our evaluations show that MJPC successfully reconciles the conflicting objectives of dynamic target tracking and payload sway suppression. The RL baseline performs poorly on hardware despite training on the system-identified model. During training, the PPO agent converges to outputting maximum velocity actions as a local optimum to the task reward function. This highlights a common limitation of RL in continuous control tasks when deployed without extensive domain randomization. Future work could explore tuning the reward function to mitigate the observed “bang-bang” control effect. The classical PID controller serves as a reactive baseline. However, its performance significantly degrades as the external disturbance induced by the motion platform increases, failing to anticipate continuous base perturbations. While the PID controller often drives the payload to reach the target position quicker, it does so at the cost of inducing more severe oscillations on the payload. Conversely, our proposed MJPC controller, deployed across both a high-

performance laptop and a resource-constrained Jetson AGX Orin, demonstrates the best overall performance with least degradation across motion platform settings. Particularly, despite having less available compute, our edge variant often matches or outperforms our high-performance variant.

B. Feasibility of Real-Time MJPC with CEM Planning

We first analyze convergence of the planner in simulation. We configure MJPC to generate plans using a varying number of CEM iterations per planning cycle, ranging from 1 to 100. For each configuration, average the nominal return (lowest trajectory cost prior to the action update) over 50 independent runs. As shown in Fig. 4, CEM demonstrates clear convergence, with the nominal cost decreasing sharply and eventually plateauing after approximately 60 iterations. However, each additional iteration linearly increases planning time (dashed black line in Fig. 4, and exceeding 10 iterations violates the 20 Hz real-time control frequency constraint).

To establish practical feasibility, we replicate this analysis on the physical hardware, restricting the range from 1 to 10 iterations. For each configuration, we deploy the controller to maintain the payload over a stationary target and record the xy position error over 1 minute. Fig. 5 shows the mean position error for SLOW, MEDIUM and FAST platform speeds. Too few iterations produce under-converged policies with high tracking error, while too many introduce latency that destabilises the system. Operating at five planning iterations strikes the balance: the resulting replanning rate (~ 40 Hz) provides sufficient policy refinement to suppress double-pendulum sway while remaining well above the crane control frequency.

C. Robustness under Model Discrepancies

Finally, we assess the MJPC crane controller’s robustness to parameter mismatch between the MuJoCo planning model and the physical system by replicating the target tracking experimental setup outlined in Section VI-A under unmodeled hardware conditions. We attach a secondary cylindrical payload (0.35 m, 0.23 kg—74% of the 0.31 kg primary payload mass) to the bottom of the first one so it can swing freely, effectively forming a triple-pendulum dynamic with an altered weight distribution. The MJPC planner continues to use the unmodified double-pendulum model, meaning both the additional mass and the extra DoF are entirely

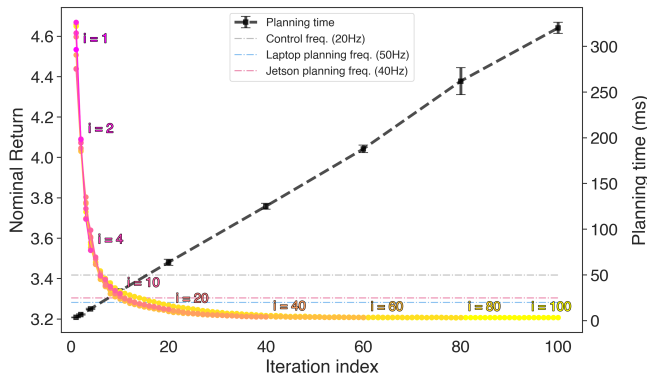


Fig. 4: Mean nominal return over 50 replications for various CEM planning iterations i in simulation. We also plot the planning time per cycle for each iteration parameter.

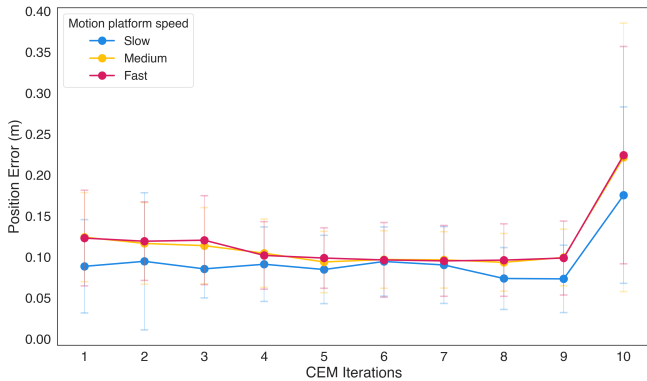


Fig. 5: Mean payload position error from target, on the real crane, over 60s interval for various CEM planning iterations.

unmodeled. Due to increased payload instability, we collect four replications per controller per platform condition.

The unmodeled secondary mass introduces two new disturbance modes: out-of-phase oscillation between primary and secondary payloads during platform acceleration, and at higher platform speed, circular swinging that induces rotational spin on the primary payload—a structural mode absent from the planning model.

Table V summarises the difference in position and angular error metrics from the single-payload setting. MJPC retains the lowest position error across all platform conditions despite an increase of 3–23 cm from the single-payload baseline. Its angular error increases most at STATIC and SLOW speeds ($+2.1^\circ$ and $+2.8^\circ$), reflecting persistent out-of-phase oscillation between the two payloads. At FAST platform speed, circular swinging of the secondary payload was observed more frequently, occasionally developing into sustained spin that interrupted individual trials.

PID shows the smallest angular degradation across conditions, with sway performance *improving* at MEDIUM and FAST speeds (deltas of -1.39° and -0.52°) relative to the nominal case, as its conservative, low-bandwidth actuation avoids exciting the secondary pendulum mode, allowing the additional mass to act as passive damping on the primary payload. However, this comes at the cost of increased

station-keeping error (6–15 cm above the nominal baseline), a degradation not observed in the single-payload experiments.

RL exhibits the largest degradation across all conditions, with position error increasing by 0.35–0.48 m and angular error by 0.27 – 3.86° relative to the nominal case, compounding already high baseline errors. The learned policy, trained on nominal payload dynamics, fails to adapt to the added complexity in the system dynamics.

Despite severe model mismatch – 74% unmodeled payload mass increase and an absent DoF – MJPC degrades gracefully: frequent replanning continuously corrects for position error through state feedback, maintaining the best target tracking across all conditions. However, the replanning cannot fully compensate for the unmodeled sway modes, with angular error roughly doubling at STATIC and SLOW speeds where the out-of-phase oscillation is most persistent.

VII. CONCLUSION AND FUTURE WORK

We present a real-time, sampling-based MPC framework for the control of a shipboard boom crane. Our approach pairs a system-identified MuJoCo model with a CEM planner to suppress double-pendulum payload sway under base perturbations. By directly evaluating candidate policies through forward rollouts in simulation, we eliminate the need for linearization, DoF reduction, or analytical model derivation common in existing crane MPC methods. Our adaptive cost function successfully reconciles the competing demands of fast payload transfer and sway suppression. Through extensive hardware experiments and ablation studies, we validate the practical deployability of this onboard MuJoCo-based MPC paradigm. The competitive performance of our controller under strict planning time constraints makes it feasible to run simulation-based planning on compute-limited industrial hardware.

Future work will address current limitations regarding disturbance prediction and sensing. To improve responsiveness to sudden aperiodic disturbances, we plan to replace the current periodic history assumption with a state estimator, such as a Kalman filter. Furthermore, to eliminate reliance on external motion capture, we will implement onboard sensor fusion using IMUs, RGB-D cameras, and LiDAR to enhance reliability in outdoor settings. Finally, we aim to extend the MuJoCo model with an additional hinge joint to capture and suppress the rotational spin of the payload about the cable axis, a dynamic currently unmodelled in the xy plane representation.

REFERENCES

- [1] J. Vaughan, D. Kim, and W. Singhose, “Control of Tower Cranes With Double-Pendulum Payload Dynamics,” *IEEE Transactions on Control Systems Technology*, vol. 18, no. 6, pp. 1345–1358, Nov. 2010. [Online]. Available: <https://ieeexplore.ieee.org/document/5422812>
- [2] L. Ramli, Z. Mohamed, A. M. Abdullahi, H. Jaafar, and I. M. Lazim, “Control strategies for crane systems: A comprehensive review,” *Mechanical Systems and Signal Processing*, vol. 95, pp. 1–23, Oct. 2017. [Online]. Available: <https://linkinghub.elsevier.com/retrieve/pii/S0888327017301425>
- [3] Y. Cao and T. Li, “Review of antiswing control of shipboard cranes,” *IEEE/CAA Journal of Automatica Sinica*, vol. 7, no. 2, pp. 346–354, Mar. 2020. [Online]. Available: <https://ieeexplore.ieee.org/document/9016392/>

- [4] T. Howell, N. Gileadi, S. Tunyasuvunakool, K. Zakka, T. Erez, and Y. Tassa, "Predictive Sampling: Real-time Behaviour Synthesis with MuJoCo," Dec. 2022, arXiv:2212.00541 [cs]. [Online]. Available: <http://arxiv.org/abs/2212.00541>
- [5] G. Rigatos, "Nonlinear Optimal Control for the Underactuated Double-Pendulum Overhead Crane," *Journal of Vibration Engineering & Technologies*, vol. 12, no. 2, pp. 1203–1223, Feb. 2024. [Online]. Available: <https://doi.org/10.1007/s42417-023-00902-y>
- [6] N. Sun, Y. Wu, Y. Fang, and H. Chen, "Nonlinear Antiswing Control for Crane Systems With Double-Pendulum Swing Effects and Uncertain Parameters: Design and Experiments," *IEEE Transactions on Automation Science and Engineering*, vol. 15, no. 3, pp. 1413–1422, Jul. 2018. [Online]. Available: <https://ieeexplore.ieee.org/document/7990578>
- [7] J. Lin, Y. Fang, B. Lu, H. Cao, and Y. Hao, "Constrained model predictive control for 3-d offshore boom cranes," *Control Engineering Practice*, vol. 142, p. 105741, 2024. [Online]. Available: <https://www.sciencedirect.com/science/article/pii/S0967066123003106>
- [8] Y. Cao and T. Li, "Nonlinear antiswing control for shipboard boom cranes with full state constraints," *Applied Ocean Research*, vol. 146, p. 103964, 2024. [Online]. Available: <https://www.sciencedirect.com/science/article/pii/S0141118724000865>
- [9] M. Richter, E. Arnold, K. Schneider, J. K. Eberharter, and O. Sawodny, "Model predictive trajectory planning with fallback-strategy for an active heave compensation system," in *2014 American Control Conference*, 2014, pp. 1919–1924.
- [10] E. Das, W. A. Welch, P. Spieler, K. Albee, A. Noca, J. Edlund, J. Beckett, T. Touma, J. Todd, S. Bhamidipati, S. Kombo, M. Saboia, A. Sabel, G. Lim, R. Thakker, A. Rahmani, and J. W. Burdick, "Safe Payload Transfer with Ship-Mounted Cranes: A Robust Model Predictive Control Approach," Oct. 2025, arXiv:2510.16953 [eess]. [Online]. Available: <http://arxiv.org/abs/2510.16953>
- [11] M. N. Vu, A. Wachter, G. Ebmer, M.-P. Ecker, T. Glück, A. Nguyen, W. Kemmetmueller, and A. Kugi, "Towards Autonomous Wood-Log Grasping with a Forestry Crane: Simulator and Benchmarking," Feb. 2025, arXiv:2502.01304 [cs]. [Online]. Available: <http://arxiv.org/abs/2502.01304>
- [12] J. Z. Zhang, T. A. Howell, Z. Yi, C. Pan, G. Shi, G. Qu, T. Erez, Y. Tassa, and Z. Manchester, "Whole-Body Model-Predictive Control of Legged Robots with MuJoCo," Oct. 2025, arXiv:2503.04613 [cs]. [Online]. Available: <http://arxiv.org/abs/2503.04613>
- [13] C. Liang and D. Rakita, "Robust and Efficient MuJoCo-based Model Predictive Control via Web of Affine Spaces Derivatives," Dec. 2025, arXiv:2512.21109 [cs]. [Online]. Available: <http://arxiv.org/abs/2512.21109>
- [14] A. H. Li, P. Culbertson, V. Kurtz, and A. D. Ames, "DROP: Dexterous Reorientation via Online Planning," in *2025 IEEE International Conference on Robotics and Automation (ICRA)*, May 2025, pp. 14 299–14 306. [Online]. Available: <https://ieeexplore.ieee.org/abstract/document/11128433>
- [15] A. Hess, A. M. Kübler, B. Forrai, M. Dogar, and R. K. Katzschmann, "Sampling-Based Model Predictive Control for Dexterous Manipulation on a Biomimetic Tendon-Driven Hand," in *2025 IEEE/RSJ International Conference on Intelligent Robots and Systems (IROS)*, Oct. 2025, pp. 5509–5516, iSSN: 2153-0866. [Online]. Available: <https://ieeexplore.ieee.org/abstract/document/11246473>
- [16] K. Zakka, Y. Tassa, and MuJoCo Menagerie Contributors, "MuJoCo Menagerie: A collection of high-quality simulation models for MuJoCo," 2022. [Online]. Available: http://github.com/google-deeppmind/mujoco_menagerie
- [17] K. Shaw, A. Agarwal, and D. Pathak, "Leap hand: Low-cost, efficient, and anthropomorphic hand for robot learning," 2023. [Online]. Available: <https://arxiv.org/abs/2309.06440>
- [18] R. Rubinstein, "The cross-entropy method for combinatorial and continuous optimization," *Methodology And Computing In Applied Probability*, vol. 1, no. 2, pp. 127–190, Sep 1999. [Online]. Available: <https://doi.org/10.1023/A:1010091220143>
- [19] W. Tang, R. Ma, W. Wang, and H. Gao, "Optimization-Based Input-Shaping Swing Control of Overhead Cranes," *Applied Sciences*, vol. 13, no. 17, p. 9637, Jan. 2023. [Online]. Available: <https://www.mdpi.com/2076-3417/13/17/9637>
- [20] W. Tang, E. Zhao, L. Sun, and H. Gao, "An active swing suppression control scheme of overhead cranes based on input shaping model predictive control," *Systems Science & Control Engineering*, vol. 11, no. 1, p. 2188401, Dec. 2023. eprint: <https://doi.org/10.1080/21642583.2023.2188401>. [Online]. Available: <https://doi.org/10.1080/21642583.2023.2188401>
- [21] G. Li, X. Ma, J. Li, and Y. Li, "Sliding Mode Control for Tower Crane with Double Spherical Pendulum and Variable Cable Length," in *2024 3rd Conference on Fully Actuated System Theory and Applications (FASTA)*, May 2024, pp. 1017–1022. [Online]. Available: <https://ieeexplore.ieee.org/abstract/document/10595392>
- [22] G. Li, X. Ma, and Y. Li, "Adaptive Anti-Swing Control for 7-DOF Overhead Crane With Double Spherical Pendulum and Varying Cable Length," *IEEE Transactions on Automation Science and Engineering*, vol. 21, no. 4, pp. 5240–5251, Oct. 2024. [Online]. Available: <https://ieeexplore.ieee.org/document/10239216>
- [23] J. Huang, W. Wang, and J. Zhou, "Adaptive Control Design for Underactuated Cranes With Guaranteed Transient Performance: Theoretical Design and Experimental Verification," *IEEE Transactions on Industrial Electronics*, vol. 69, no. 3, pp. 2822–2832, Mar. 2022. [Online]. Available: <https://ieeexplore.ieee.org/abstract/document/9381605>
- [24] M. Böck and A. Kugi, "Real-time nonlinear model predictive path-following control of a laboratory tower crane," *IEEE Transactions on Control Systems Technology*, vol. 22, no. 4, pp. 1461–1473, 2014.
- [25] Y. Cao, T. Li, and L.-Y. Hao, "Lyapunov-based model predictive control for shipboard boom cranes under input saturation," *IEEE Transactions on Automation Science and Engineering*, vol. 20, no. 3, pp. 2011–2021, 2023.
- [26] G. O. Tysse, A. Cibicik, L. Tingelstad, and O. Egeland, "Lyapunov-based damping controller with nonlinear mpc control of payload position for a knuckle boom crane," *Automatica*, vol. 140, p. 110219, 2022. [Online]. Available: <https://www.sciencedirect.com/science/article/pii/S0005109822000644>
- [27] T. Kuszniar and J. Smoczek, "Nonlinear model predictive control with evolutionary data-driven prediction model and particle swarm optimization optimizer for an overhead crane," *Applied Sciences*, vol. 14, no. 12, 2024. [Online]. Available: <https://www.mdpi.com/2076-3417/14/12/5112>
- [28] J.-G. Jang and S.-H. Ham, "Anti-swing overhead crane control algorithm based on multi-body dynamics using reinforcement learning," *International Journal of Naval Architecture and Ocean Engineering*, vol. 18, p. 100719, 2026. [Online]. Available: <https://www.sciencedirect.com/science/article/pii/S2092678225000779>
- [29] J. Zhong, D. Nikovski, W. S. Yezunis, and T. Ando, "Learning Time-Optimal Control of Gantry Cranes," in *2024 International Conference on Machine Learning and Applications (ICMLA)*, Dec. 2024, pp. 945–950, iSSN: 1946-0759. [Online]. Available: <https://ieeexplore.ieee.org/abstract/document/10903464>
- [30] S. Akki and T. Chen, "Benchmarking Model Predictive Control and Reinforcement Learning-Based Control for Legged Robot Locomotion in MuJoCo Simulation," *IEEE Access*, vol. 13, pp. 108 732–108 742, 2025. [Online]. Available: <https://ieeexplore.ieee.org/abstract/document/11048516>
- [31] T. Erez, K. Lowrey, Y. Tassa, V. Kumar, S. Kolev, and E. Todorov, "An integrated system for real-time model predictive control of humanoid robots," in *2013 13th IEEE-RAS International Conference on Humanoid Robots (Humanoids)*, 2013, pp. 292–299.
- [32] J. Alvarez-Padilla, J. Z. Zhang, S. Kwok, J. M. Dolan, and Z. Manchester, "Real-Time Whole-Body Control of Legged Robots with Model-Predictive Path Integral Control," in *2025 IEEE International Conference on Robotics and Automation (ICRA)*, May 2025, pp. 14 721–14 727. [Online]. Available: <https://ieeexplore.ieee.org/document/11128271>
- [33] C. Pezzato, C. Salmi, E. Trevisan, M. Spahn, J. Alonso-Mora, and C. H. Corbato, "Sampling-based Model Predictive Control Leveraging Parallelizable Physics Simulations," Jan. 2025, arXiv:2307.09105 [cs]. [Online]. Available: <http://arxiv.org/abs/2307.09105>
- [34] B. Riviere and J. W. Burdick, "Optimal noise control of sampling-based predictive control for inference time scaling," in *Second Workshop on Out-of-Distribution Generalization in Robotics at RSS 2025*, 2025. [Online]. Available: <https://openreview.net/forum?id=j41jE8GBYJ>
- [35] J. Schulman, F. Wolski, P. Dhariwal, A. Radford, and O. Klimov, "Proximal policy optimization algorithms," *arXiv preprint arXiv:1707.06347*, 2017.
- [36] H. B. Mann and D. R. Whitney, "On a test of whether one of two random variables is stochastically larger than the other," *The annals of mathematical statistics*, pp. 50–60, 1947.